Int. J. Electrochem. Sci., 16 **(2021)** Article ID: 210550, doi: 10.20964/2021.05.06

International Journal of
ELECTROCHEMICAL
SCIENCE
www.electrochemsci.org

A non-enzymatic Electrochemical Sensor Based on rGO-PPy for Rapid and Sensitive Determination of Histamine in Meat

Bobo Hu[1], *Nana Zhang*[2], *Huihui Li*[1,*], *Chong Sun*[2,3,*]

[1] Jiangsu Collaborative Innovation Centre of Biomedical Functional Materials, Jiangsu Key Laboratory of Biomedical Materials, School of Chemistry and Materials Science, Nanjing Normal University, Nanjing 210023, PR China
[2] Institute of Agricultural Products Processing, Jiangsu Academy of Agricultural Sciences, Nanjing 210014, PR China
[3] Jiangsu Key Laboratory for Food Quality and Safety-State Key Laboratory Cultivation Base of Ministry of Science and Technology, Nanjing 210014, PR China
[*]E-mail: huihuili@njnu.edu.cn (H.H. Li); sunchong@jaas.ac.cn (C. Sun)

Received: 10 December 2020 / *Accepted:* 8 February 2021 / *Published:* 31 March 2021

Sensitive and reliable quantification of histamine (His) is essential to ensure food safety. In this study, a sensing material consisting of reduced graphene oxide/polypyrrole (rGO-PPy) composites is successfully prepared by a two-step synthesis method and verified by transmission electron microscopy (TEM), Fourier transform infrared (FTIR) spectroscopy, ultraviolet-visible (UV-vis) spectroscopy, X-ray diffraction (XRD) and X-ray photoelectron spectroscopy (XPS). Based on rGO-PPy, an electrochemical method is established, and the electrochemical behaviours are studied by cyclic voltammetry (CV), electrochemical impedance spectroscopy (EIS) and differential pulse voltammetry (DPV). The experimental parameters, such as the detection method, the concentration and volume of rGO-PPy modified on GCE, and the pH value of the buffer solution, are optimized. Under the optimized conditions, the linear equation of the electrochemical sensor to His is I (μA) = 0.01047c + 0.1842 (R^2 = 0.9970) with a linear range of 10~800 μM, and the detection limit is 3.01 μM. Practical samples are also detected, which proves that the sensor has great application prospects. Therefore, this idea and method will make an excellent contribution to food safety.

Keywords: rGO-PPy; Histamine; Electrochemical sensor; Food safety

1. INTRODUCTION

Histamine (His) is a toxic organic compound with a low molecular weight that is widely distributed in livestock meat, fish, alcoholic beverages and other foods [1-3]. Moreover, it is also considered to be an indicator of food spoilage during storage [1, 2], and a high concentrations of His in spoiled foods can cause allergic reactions [3], asthma [4], irritable bowel syndrome [5], arthritis [6-8] and other diseases. The production of His in aquatic products is closely related to the degradation of free histidine under the action of microbial histidine decarboxylase [9]. The European Union (EU) stipulates that the content of His in fish should not exceed 200 $mg \cdot kg^{-1}$ [10-12] and should not exceed 100 $mg \cdot kg^{-1}$ in other foods [13].

Many His detection methods have been developed, such as gas chromatography-mass spectrometry (GC-MS) [14], high-performance liquid chromatography coupled with mass spectrometry (HPLC-MS) [15], high-performance liquid chromatography coupled with UV-vis spectroscopy [16, 17] and thin-layer chromatography/densitometry [18]. However, these methods have the disadvantages of a high cost, complicated operation and long detection time; thus, they cannot meet practical application requirements. Electrochemistry has the advantages of being a low cost, easy operation that utilizes inexpensive equipment and demonstrates reliability, a fast response, short analysis time, high sensitivity and good selectivity [19-21]. Leonardo and Campàs developed an electrochemical biosensor based on diamine oxidase (DAO) combined with magnetic beads (MBs), which can be applied in detecting multiple biogenic amines (BAs) [22]. Telsnig et al. designed a screen-printed carbon electrode grafted with MnO_2, and pea seedling amine oxidase was modified on the electrode. The sensor was applied for the rapid and sensitive detection of BAs in chickens [23]. However, enzyme sensors have the disadvantages of instability and complex modification procedures [24]. Therefore, it is necessary to establish an enzyme-free electrochemical method for the rapid detection of His in practical samples.

Graphene oxide (GO) has the characteristics of a large specific surface area, good biocompatibility and low cost [25-27]. However, the GO surface contains a high content of oxygen-containing groups (carboxyl groups, epoxy groups, etc.), resulting in unsatisfactory conductivity [28]. To improve the performance of GO, reduced graphene oxide (rGO) was synthesized. Polypyrrole (PPy) has the characteristics of easy preparation and good conductivity and can be widely used in sensing materials, electronic instruments and other fields [29]. rGO-PPy composites form due to the electrostatic and π-π interactions between rGO and PPy [25]. The rGO-PPy composites are expected to present all the advantageous properties of the two kinds of materials. Subsequently, the rGO-PPy composites were immobilized on the surface of a glass carbon electrode (GCE), and an electrochemical sensor was established for the measurement of His. Experimental results show that His undergoes an oxidation reaction on the sensor in alkaline phosphate-buffered saline (PBS, pH = 12.0). According to the relationship between the concentrations and current signals, the quantitative detection of His can be achieved. Therefore, the development of the sensor has good application prospects in the field of food safety.

2. EXPERIMENT

2.1. Chemicals and regents

GO was obtained from Xianfeng Nano Material Technology Co., Ltd. His putrescine (Put), spermine (Spm), spermidine (Spd) and phenethylamine (Pea) were purchased from Aladdin Bio-Chem Technology Co., Ltd. (Shanghai, China). Ferric chloride hexahydrate ($FeCl_3 \cdot 6H_2O$), disodium hydrogen phosphate dodecahydrate (Na_2HPO_4), potassium dihydrogen phosphate (KH_2PO_4), pyrrole, ethanol, ammonia ($NH_3 \cdot H_2O$), hydrazine hydrate, sodium hydroxide (NaOH), potassium chloride (KCl) and hydrochloric acid (HCl) were supplied by Sinopharm Chemical Regent Co., Ltd. Cadaverine (Cad) and L-glutamic acid (Glu) were purchased from Sigma-Aldrich (USA). All chemicals were analytical reagents, and all solutions were prepared by ultrapure water.

2.2. Synthesis of rGO-PPy

The synthesis procedure of rGO-PPy was divided into two steps. First, GO-PPy was synthesized through a simple in situ route, followed by a reduction reaction to obtain rGO-PPy. Specifically, 10.0 mL of GO (1.0 $mg \cdot mL^{-1}$) suspension was sonicated for 10.0 min. Then, 150.0 μL of pyrrole dissolved in ethanol was added and sonicated for 0.5 h. After the addition of 10.0 mL $FeCl_3$ (0.5 $mol \cdot L^{-1}$), the mixed solution was continuously stirred for 24.0 h to obtain GO-PPy by oxidative polymerization. Afterward, GO-PPy was washed with ultrapure water and ethanol to remove excess pyrrole and dried under vacuum at 60 °C to obtain GO-PPy.

The rGO-PPy material was prepared as follows. GO-PPy (10.0 mL, 1.0 $mg \cdot mL^{-1}$) was mixed with 100.0 μL of $NH_3 \cdot H_2O$ and 20.0 μL of hydrazine hydrate, and then the solution was refluxed at 60.0 °C for 16.0 h. After that, the obtained solution was washed with ultrapure water and ethanol. Finally, the purified rGO-PPy was dried under vacuum at 60.0 °C.

2.3. Apparatus and instruments

The morphology and structure of the rGO-PPy nanomaterial was observed with transmission electron microscopy (TEM, HITACHI H-7650, Japan) at an accelerating voltage of 80 kV. Fourier transform infrared (FTIR, VARIAN Cary 5000, USA) spectroscopy, ultraviolet visible (UV-*vis*, Cary 50 Conc, Australia) spectroscopy, X-ray diffraction (XRD, Rigaku, Japan) and X-ray photoelectron spectroscopy (XPS, Thermo ESCALAB250Xi, USA) were used to characterize the successful synthesis of rGO-PPy.

2.4 Process of electrode modification and measurement

The GCE (surface area was approximately 0.078 cm^2) was polished with 0.3 and 0.05 μm alumina slurries, washed with ultrapure water and ethanol and dried with nitrogen. Then, 7.0 μL of an

rGO-PPy (4.0 mg·mL^{-1}) suspension solution was modified on the electrode surface and dried under natural conditions for later use.

The electrochemical measurements were performed on a CHI760E electrochemical workstation (Shanghai, China). The electrochemical system involved in this subject used a three-electrode system, in which the GCE was used as the working electrode, platinum wire (Pt) was used as the auxiliary electrode and a saturated calomel electrode (SCE) was used as the reference electrode. The electrochemical experiments mainly included cyclic voltammetry (CV), electrochemical impedance spectroscopy (EIS) and differential pulse voltammetry (DPV). The CV test was conducted in a mixed solution containing 1.0 mM $[Fe(CN)_6]^{3-/4-}$ (1:1) and 0.1 M KCl with a potential range of -0.2 to 0.7 V. The EIS test was performed in a 5.0 mM $[Fe(CN)_6]^{3-/4-}$ solution containing 0.1 M KCl with an amplitude of 5.0 mV and a frequency range of 1 to 100 kHz. DPV was performed in 0.1 M PBS (pH = 12.0) with a voltage range of 0.4~0.9 V.

2.5. Detection of real samples

Fish meat was purchased from a local supermarket. Briefly, 2.0 g of fish was added into 8.0 mL of 0.4 M perchloric acid (pH = 7.4) and stirred for 1 min. The mixture was centrifuged, and the supernatant was collected. Then, 10.0 mL of n-hexane was added to 10.0 mL of the extract and stirred for 5.0 min. After that, the organic phase was removed with the help of a rotary evaporation apparatus. The extract was used in the following experiment.

3. RESULTS AND DISCUSSION

3.1 Characterization of the rGO-PPy composites

The morphological character of rGO-PPy was investigated by TEM. As shown in Figure 1A, rGO had a two-dimensional sheet structure with a wrinkled shape [30]. In Figure 1B, rGO was in the form of flakes, and PPy was evenly dispersed on the rGO, which indicated that rGO-PPy was successfully synthesized.

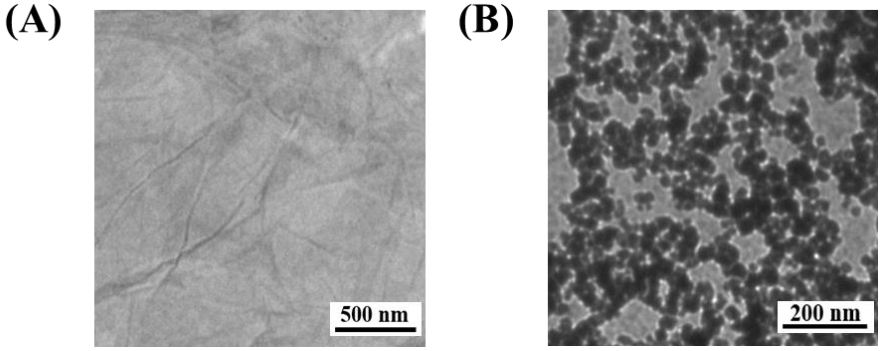

Figure 1. (A) TEM image of rGO and (B) TEM image of rGO-PPy.

Figure 2A shows the FTIR spectra of rGO (curve a), PPy (curve b) and rGO-PPy (curve c). In curve a, the characteristic peaks of oxygen-containing functional groups were located at 1451 cm^{-1} and 1050 cm^{-1}, which were attributed to the C-OH and C-O stretching vibrations of rGO, respectively [31]. Moreover, the peaks at 1630 cm^{-1} and 3440 cm^{-1} were associated with the -OH and C=C stretching vibrations of rGO, respectively [32]. In curve b, the absorption peaks at 3430 cm^{-1} and 1315 cm^{-1} originated from the N-H and C-N stretching vibrations of PPy, respectively [31, 33-35]. The peaks at 1462 cm^{-1} and 1550 cm^{-1} were due to C=C stretching vibrations, and the broadband peak at 1306 cm^{-1}~917 cm^{-1} was attributed to the in-and-out of plane C-H mode of the PPy polymer chains [30]. Both the characteristic peaks of rGO and PPy could be found in curve c, which confirmed the existence of rGO-PPy.

XRD patterns were used to characterize the structure and chemical states of rGO-PPy (Figure 2B). The strong diffraction peak at 2θ=11.0° was the characteristic peak of the GO(001) plane (curve a) [36]. Regarding rGO (curve b), the (001) peak disappeared, and a broad peak at 23.4° appeared, which indicated that the reduction of GO was successful [37]. Furthermore, it was found that rGO-PPy (curve c) composites exhibited a new peak at 25.1°, representing the existence of PPy [28]. Moreover, the broad peak at 23.4° disappeared in the XRD pattern of rGO-PPy, which was attributed to rGO being used as a substrate for PPy [38].

Moreover, XPS was used to determine the chemical states of rGO-PPy. Figure 2C shows the characteristic signature of C, O and N, which accounted for 70.66%, 14.57% and 14.78%, respectively. In this case, O was from rGO, whereas N was related to the existence of PPy [39]. In Figure 2D, the C 1s spectrum showed O 1s peaks at 284.45 eV (C-C/C=C), 285.5 eV (C-N), 285.85 eV (C-O) and 288.25 eV (C-N) [35, 40]. The peaks at 285.5 eV (C-N) indicated that PPy was successfully fixed onto the surface of rGO [40, 41].

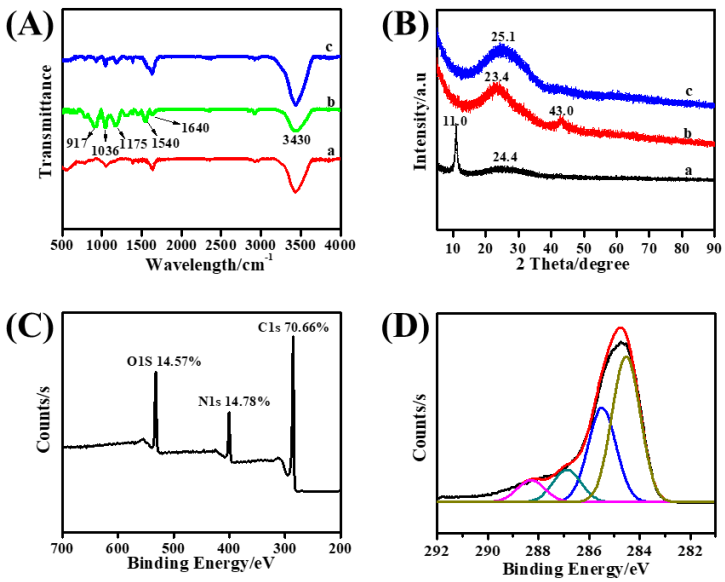

Figure 2. (A) FTIR spectra of (a) rGO, (b) PPy and (c) rGO-PPy; (B) XRD patterns of (a) GO, (b) rGO and (c) rGO-PPy; (C) XPS spectra of rGO-PPy; and (D) C 1s spectrum of rGO-PPy.

3.2. Electrochemical behaviour of the modified electrode

CV was conducted to investigate the electrochemical properties of different materials. Figure 3A shows the CV curves of (a) GO/GCE, (b) GO-PPy/GCE and (c) rGO-PPy/GCE. Compared with GO/GCE (curve a), a stronger oxidation peak current was shown in GO-PPy/GCE (curve b), which was due to the better conductivity of GO-PPy. When GO was reduced to rGO, the peak current increased further (curve c), which was attributed to the large amount of oxygen-containing groups on GO disappearing and the electron interfacial transfer speed increasing.

The surface characteristics of the sensor were further studied by EIS. The charge transfer resistance (R_{et}) was obtained by using the diameter of the semicircle formed by the Nyquist diagram [42]. The greater the R_{et} obtained, the larger the semicircle diameter was. Figure 3B shows the EIS spectra of different modified electrodes: (a) GO/GCE, (b) GO-PPy/GCE and (c) rGO-PPy/GCE. From Figure 3B, it could be observed that there was a smaller semicircle in the low-frequency region, proving that the conductivity of GO-PPy/GCE was better than that of GO/GCE. The semicircle of rGO-PPy/GCE appeared in the lowest frequency region, which indicated that rGO could enhance conductivity.

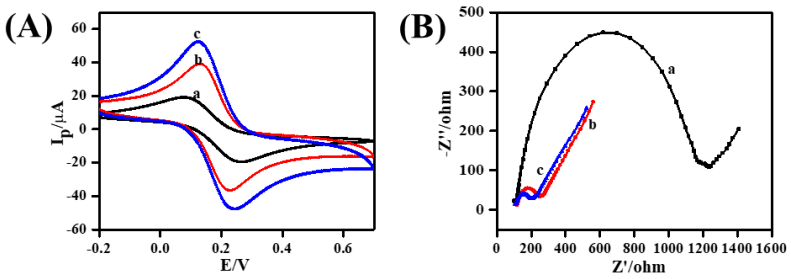

Figure 3. (A) CV plots of different electrodes: (a) GO/GCE, (b) GO-PPy/GCE, and (c) rGO-PPy/GCE in a 1.0 mM $[Fe(CN)_6]^{3-/4-}$ (1:1) solution containing 0.1 M KCl at a scan rate of 100.0 $mV \cdot s^{-1}$ and (B) EIS curves of (a) GO/GCE, (b) GO-PPy/GCE, and (c) rGO-PPy/GCE in a 5.0 mM $[Fe(CN)_6]^{3-/4-}$ (1:1) solution containing 0.1 M KCl (pH = 7.0).

3.3 Electrochemical mechanism for detecting histamine with rGO-PPy/GCE

His can be oxidized by substances such as Ag_2O and DAO [24]. In Figure 4A, it could be observed that there was no oxidation peak on rGO/GCE, which indicated His could not be oxidized. However, an oxidation peak with a potential of 0.67 V was observed on PPy/GCE due to the oxidizing property of PPy [25, 43]. rGO-PPy/GCE exhibited a larger response peak than PPy/GCE, which was due to the synergistic effect of rGO and PPy in promoting electron transfer [44]. Moreover, rGO-PPy had better dispersibility than PPy (Figure S1), which proved that rGO-PPy exhibited better stability than PPy [45]. In Figure 4B, it can be observed that the response current of PPy towards His remained 21.43% ± 0.21 after ten scanning cycles, while the response current of rGO-PPy remained 96.53% ± 0.07. These results indicated that rGO-PPy was suitable for use as an electrode material for the detection of His.

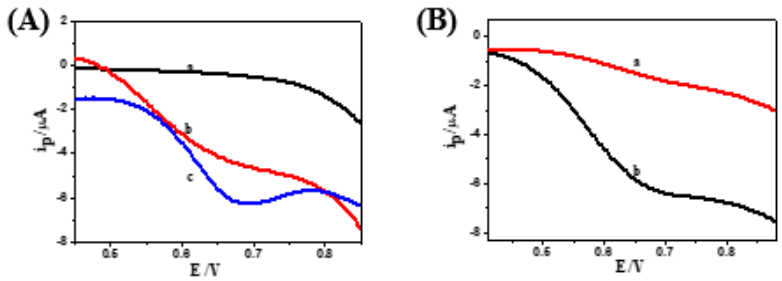

Figure 4. (A) DPV plots of different electrodes: (a) rGO/GCE, (b) PPy/GCE, and (c) rGO-PPy/GCE in a His solution (100.0 μM) and (B) DPV plots of different electrodes: (a) PPy/GCE and (b) rGO-PPy/GCE. PPy/GCE and rGO-PPy/GCE were scanned for ten cycles between 0.4 and 0.9 V in a PBS (pH = 12.0) solution containing His (100.0 μM).

3.4 Optimization of the experimental parameters

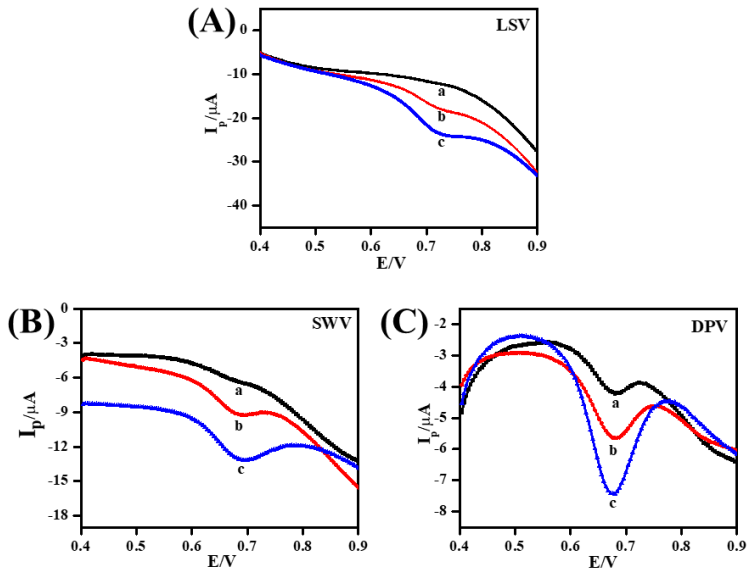

Figure 5. Influence on the determination of His (50.0 μM, 100.0 μM, and 300.0 μM) using different techniques in 0.1 mM PBS (pH = 12.0): (A) LSV (scan rate of 100.0 $mV \cdot s^{-1}$); (B) SWV; and (C) DPV.

To improve the sensitivity of the sensor, electrochemical techniques were optimized in this experiment. The current responses of LSV (Figure 5A), DPV (Figure 5B) and SWV (Figure 5C) are shown in Figure 5. The DPV technique exhibited the largest current response to His. Table 1 lists the current response of different detection methods to His. It was shown that the current signal obtained by

DPV was more sensitive than LSV and SWV. Therefore, DPV was chosen to detect His in this experiment.

Table 1. Comparison of the different electrochemical techniques for the determination of His.

His (μM)	LSV	SWV	DPV
50.00	0.226±0.05 μA	0.234±0.04 μA	0.869±0.08 μA
100.00	0.985±0.03 μA	0.934±0.07 μA	1.503±0.06 μA
300.00	2.305±0.10 μA	2.214±0.05 μA	3.705±0.09 μA

The experimental conditions, including the volume of rGO-PPy, the concentration of rGO-PPy and the pH of the electrolyte solution, were investigated by the DPV method. Figure 6A shows that the concentration of the rGO-PPy-modified electrode varied from 1.0 to 5.0 mg·mL^{-1}. The current response reached a maximum at 4.0 mg·mL^{-1} and then decreased because a massive amount of rGO-PPy accumulated on the surface of the sensor. Thus, the concentration of rGO-PPy was adjusted to 4.0 mg·mL^{-1} for the following experiments. Figure 6B shows the optimization of the amount of rGO-PPy modified on the electrode. When the amount of rGO-PPy was 7.0 μL, the current response reached the maximum, which indicated that the effective area of the electrode was completely covered. Therefore, the optimal volume of 7.0 μL was selected. To optimize the pH, different solutions with pH values ranging from 9.0 to 13.0 were prepared. As shown in Figure 6C, when the pH value increased, the current response gradually increased. Thus, a pH value of 12.0 was finally selected as the buffer solution.

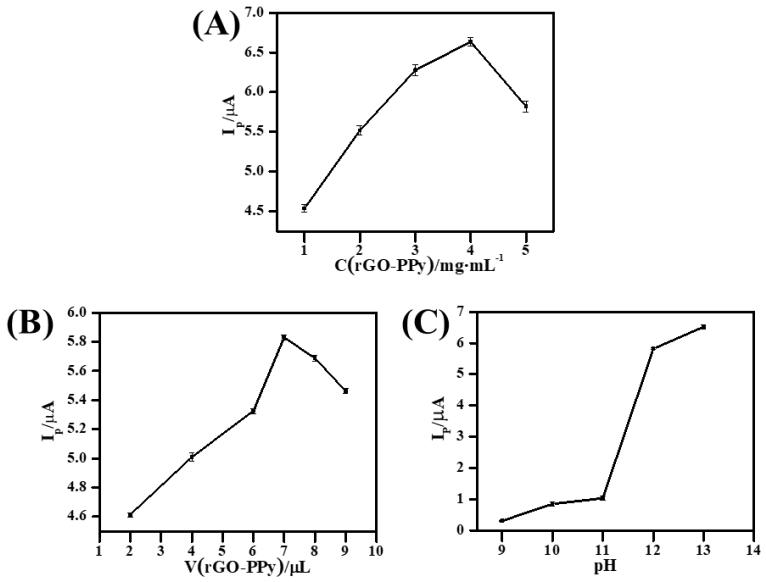

Figure 6. (A) Effects of the concentration (1.0, 2.0, 3.0, 4.0, and 5.0 mg·mL^{-1}) of rGO-PPy; (B) effects of volume (2.0, 4.0, 6.0, 7.0, 8.0, and 9.0 μL) of rGO-PPy modified on the electrode; and (C) effects of the buffer pH (9.0, 10.0, 11.0, 12.0, and 13.0). The scan rate was100.0 mV·s^{-1}.

3.5. Effects of the scan rate

Figure 7A shows the CVs of rGO-PPy/GCE obtained at different scan rates ranging from 20.0 to 200.0 $mV \cdot s^{-1}$. The linear equation was I (μA) = 0.0357v + 2.0652 (R^2 = 0.9941) (Figure 7B). The current value was proportional to the sweep rate, which indicated that the adsorption control process occurred on the electrode surface.

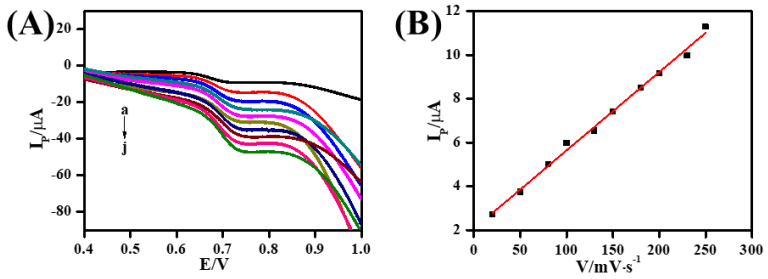

Figure 7 (A) LSV plots of rGO-PPy/GCE at different scan rates (20.0, 40.0, 60.0, 80.0, 100.0, 120.0, 140.0, 160.0, 180.0, and 200.0 $mV \cdot s^{-1}$) for the detection of His (500.0 μM) in 0.1 M PBS (pH=12.0) and (B) the variation of the anodic peak currents $mV \cdot s^{-1}$.

3.6 Electrochemical determination of His

Under the optimal experimental conditions, the linearity of His was detected. As shown in Figure 8A, the electrochemical signals increased accordingly with an increasing His concentration. The linear equation was I (μA) = 0.01047c + 0.1842 (R^2 = 0.9970), with a linear range from 10.0 to 800.0 μM and a detection limit of 3.01 μM (Figure 7B). Table 2 lists the comparison of the performance parameters of different sensors for His detection. Telsnig et al. prepared SPCE electrodes to quantify His by detecting hydrogen peroxide after His was catalysed by pea seedling amine oxidase [23]. Stojanović et al. used a carbon paste electrode modified with single-walled carbon nanotubes to determine His by voltammetry [46]. Gumpu et al. prepared CeO_2-PANI core-shell nanoparticles by a hydrothermal method. DAO was immobilized on CeO_2-PANI/GCE to detect His [48]. Leonardo and Campàs successfully prepared DAO-MB biosensors, and the biosensors were used to determine BAs (His, Cad, and Put) in spoiled fish samples [22]. Hadi and Mostaanzadeh prepared a His sensor using Ni-based metallogenic framework (Ni-BTC, BTC = 1,3,5-benzenetricarboxylate) crystals and multiwalled carbon nanotubes. This sensor was used to quantitatively determine His in human urine samples [47]. In this work, rGO-PPy was successfully synthesized, and the method was rather simple. Based on the good conductivity and biocompatibility of rGO-PPy, the His sensor was fabricated without an enzyme. Compared with other electrochemical methods, the prepared sensor exhibited higher sensitivity, a larger detection range and a lower detection limit to His.

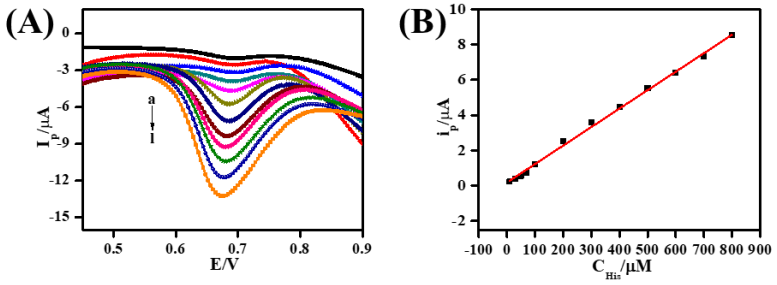

Figure 8. (A) DPV plots of rGO-PPy/GCE in 0.1 M PBS (pH = 12.0) obtained from various concentrations of His (10.0, 30.0, 50.0, 70.0, 100.0, 200.0, 300.0, 400.0, 500.0, 600.0, 700.0, and 800.0 μM). The scan rate was 100.0 $mV \cdot s^{-1}$. (B) Plot of the peak currents as a function of His.

Table 2. Comparison of the different methods for the detection of His.

Sensor	R^2	Linear range	Detection limit	References
SPCE	0.9807	10~300 μM	3.0 μM	[23]
SWCNT/CPE	0.9968	4.5~720 μM	1.26 μM	[46]
DAO/CeO_2-PANI/GCE	0.9914	450~1050 μM	48.7 μM	[48]
DAO-MBs biosensors	0.9980	0.06~1 mM	8.25 μM	[22]
Ni-BTC/CNT/GCE	0.9967	1~160 μM	0.41 μM	[47]
rGO-PPy/GCE	0.9970	10~800 μM	3.01 μM	This work

3.7. Specificity, stability and reproducibility of the fabricated sensor

The specificity of the sensor was determined by incubating it with different kinds of biogenic amines (Cad, Put, Spm, Spd, Pea, and Glu). At present, enzyme immobilization methods (DAO, etc.) have been used to catalyse His. However, many substances, such as Cad and Put, could also be oxidized [49]. In this work, PPy was used as the oxidant to detect His. As shown in Figure 9, these biogenic amines had no significant interference for the detection of His, illuminating that the rGO-PPy/GCE sensor could be used for the detection of His in practical samples due to its good anti-interference ability. To verify the repeatability of the sensor, ten electrodes with the same modification process were used to detect His under the same conditions. The relative standard deviation was 5.36%, which showed that the sensor had excellent detection reproducibility. After storage at 4.0 °C for ten days, the response current value of the sensor to His remained at 94.35%. The results indicated that the sensor constructed in this experiment had excellent stability.

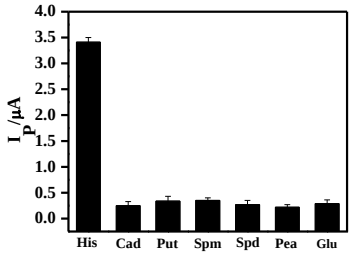

Figure 9 Anti-interference detection of rGO-PPy/GCE in 0.1 M PBS (pH = 12.0) with His (300.0 μM), Cad (3.0 mM), Put (3.0 mM), Spm (3.0 mM), Spd (3.0 mM), Pea (3.0 mM) and Glu (3.0 mM).

3.8 Real sample analysis

The feasibility of the designed sensor was evaluated by the standard addition method. Different concentrations of His were added to fish samples, and then His was extracted and detected. The results were summarized in Table 3. It could be concluded that the recovery rate measured by the sensor was 97.4%~101.2% and the RSD was less than 5%. These results proved that this method could be used for the detection of His in practical samples.

Table 3 Spiking experiment of histamine in an actual sample.

Sample	Added (μM)	Found (μM)	Recovery (%)	RSD (n = 3)
	50.0	48.7	97.4	4.7%
Fish	200.0	202.3	101.2	3.3%
	400.0	397.2	99.3	2.6%

4. CONCLUSIONS

In summary, a novel sensor based on rGO-PPy was fabricated. The sensor had good electrochemical performance and could be used for His detection. The linear equation was I (μA) = 0.01047c + 0.1842 (R^2 = 0.9970), with a linear range from 10.0 to 800.0 μM and a detection limit of 3.01 μM. The standard addition method was used to detect actual samples, the recovery rate was 97.4%~101.2%, and the RSDs were less than 5.0%. The results show that the sensor is a promising platform for the direct detection of His.

SUPPORTING MATERIALS

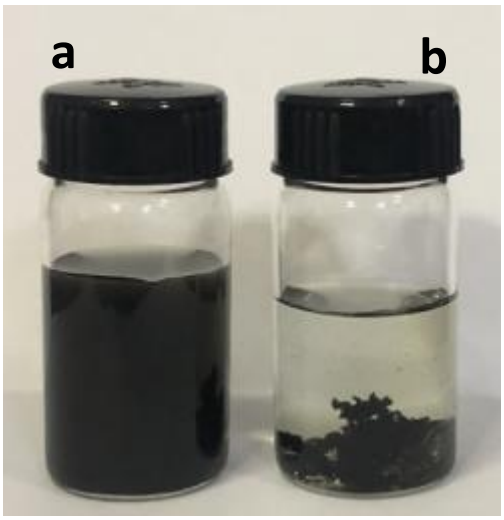

Figure S1. (a) rGO-PPy (b) PPy.

ACKNOWLEDGMENTS

This study was supported by the National Natural Science Foundation of China (21977050) and the Independent Research Project of Jiangsu Key Laboratory for Food Quality and Safety (2019JG001).

References

1. F. Bedia Erim, *Trends Anal. Chem.,* 52 (2013) 239.
2. V. Venugopal, *Biosens. Bioelectron.,* 17 (2002) 147.
3. M.V. White, *J.Allergy Clin. Immun.,* 86 (1990) 599.
4. P.J. Dunford and S.T. Holgate, *Histamine in Inflammation,* R.L. Thurmond, (2010) Springer US, Boston.
5. A. Fabisiak, J. Włodarczyk, N. Fabisiak, M. Storr and J. Fichna, *J. Neurogastroenterol. Motil.,* 23 (2017) 341-348.
6. X.D. Yang, W. Ai, S. Asfaha, G. Bhagat, R.A. Friedman, G. Jin, H. Park, B. Shykind, T.G. Diacovo, A. Falus and T.C. Wang, *Nat. Med.,* 17 (2011) 87.
7. R. Jacob, J.E. Merritt, T.J. Hallam and T.J. Rink, *Nature,* 335 (1988) 40.
8. B. Gottschalk, C. Klec, G. Leitinger, E. Bernhart, R. Rost, H. Bischof, C.T. Madreiter-Sokolowski, S. Radulović, E. Eroglu, W. Sattler, M. Waldeck-Weiermair, R. Malli and W.F. Graier, *Nat. Commun.,* 10 (2019) 3732.
9. M. Kanki, T. Yoda, T. Tsukamoto, E. Baba, *Appl. Environ. Microbiol.,* 73 (2007) 1467.
10. M. Rhoda, R.M. Simora and E. Peralta, *Asian Fish. Sci.,* 31 (2018).
11. F. Adams, F. Nolte, J. Colton, J. De Beer and L. Weddig, *J. Food Prot.,* 81 (2018) 444.
12. S. Shukla, H.-K. Park, J.-S. Lee, J.-K. Kim and M. Kim, *Food Control,* 42 (2014) 181.
13. J.A. Heyns and D.G. Kröger, *Appl. Therm. Eng.,* 30 (2010) 492.
14. C. Almeida, J.O. Fernandes and S.C. Cunha, *Food Control,* 25 (2012) 380.
15. E. Zanardi, C.G. Jagersma, S. Ghidini and R. Chizzolini, *J. Agric. Food. Chem.,* 50 (2002) 5268.
16. H. Zhai, X. Yang, L. Li, G. Xia, J. Cen, H. Huang and S. Hao, *Food Control,* 25 (2012) 303.
17. A. Pineda, J. Carrasco, C. Peña-Farfal, K. Henríquez-Aedo and M. Aranda, *Food Control,* 23 (2012) 251.

18. A. Romano, H. Klebanowski, S. La Guerche, L. Beneduce, G. Spano, M.-L. Murat and P. Lucas, *Food Chem.,* 135 (2012) 1392.
19. A. Veseli, M. Vasjari, T. Arbneshi, A. Hajrizi, Ľ. Švorc, A. Samphao and K. Kalcher, *Sens. Actuators, B,* 228 (2016) 774.
20. B.V. Sarada, T.N. Rao, D.A. Tryk and A. Fujishima, *Anal. Chem.,* 72 (2000) 1632.
21. A.-M. Iordache, R. Cristescu, E. Fagadar-Cosma, A.C. Popescu, A.A. Ciucu, S.M. Iordache, A. Balan, C. Nichita, I. Stamatin and D.B. Chrisey, *C.R. Chim.,* 21 (2018) 270.
22. S. Leonardo and M. Campàs, *Mikrochim. Acta,* 183 (2016) 1881.
23. D. Telsnig, K. Kalcher, A. Leitner and A. Ortner, *Electroanalysis,* 25 (2013) 47.
24. N. Butwong, J. Khajonklin, A. Thongbor and J.H.T. Luong, *Microchim. Acta,* 186 (2019) 714.
25. Y. Qin, B. Zhang and Z. Zhang, *Org. Electron.,* 70 (2019) 240.
26. Z. Bo, X. Shuai, S. Mao, H. Yang, J. Qian, J. Chen and J. Yan, K. Cen, *Sci. Rep,* 4 (2014) 4684.
27. J.-X. Tao, M.-C. Zhao, Y.-C. Zhao, D.-F. Yin, L. Liu, C. Gao, C. Shuai and A. Atrens, *J. Magnesium Alloys,* 8 (2020) 952.
28. G. Gnana kumar, C.J. Kirubaharan, S. Udhayakumar, K. Ramachandran, C. Karthikeyan, R. Renganathan and K.S. Nahm, *ACS Sustainable Chem. Eng.,* 2 (2014) 2283.
29. S. Ghasemi, M.R. Bari, S. Pirsa and S. Amiri, *Carbohydr. Polym.,* 232 (2020) 115801.
30. D.C. Tiwari, P. Atri and R. Sharma, *Synth. Met.,* 203 (2015) 228.
31. C. Zhu, S. Guo, Y. Fang and S. Dong, *ACS Nano,* 4 (2010) 2429.
32. B. Chitragara, W. Kim, T. Phung and D. Huh, *Polym. Compos.,* 32 (2011) 3277.
33. S. Yang, C. Shen, Y. Liang, H. Tong, W. He, X. Shi, X. Zhang and H.-j. Gao, *Nanoscale,* 3 (2011) 3277.
34. M. Singh, P. Bollella, L. Gorton, E.S. Dey and C. Dicko, *Biosens. Bioelectron.,* 150 (2020) 111859.
35. J. Chen, Y. Wang, J. Cao, Y. Liu, Y. Zhou, J.-H. Ouyang and D. Jia, *ACS Appl. Mater. Interfaces,* 9 (2017) 19831.
36. S. Park, J. An, J.R. Potts, A. Velamakanni, S. Murali and R.S. Ruoff, *Carbon*, 49 (2011) 3019.
37. G. Gnana kumar, K. Justice Babu, K.S. Nahm and Y.J. Hwang, *RSC Adv.,* 4 (2014) 7944.
38. H. Chitte, N. Bhat, V. Walunj and G. Shinde, *J. Sens. Technol.,* 1 (2011) 47.
39. M.F. Umar and A. Nasar, *Appl. Water Sci.,* 8 (2018) 211.
40. A. Berendjchi, R. Khajavi, A.A. Yousefi and M.E. Yazdanshenas, *Appl. Surf. Sci.,* 367 (2016) 36.
41. B. Zheng, T. Huang, L. Kou, X. Zhao, K. Gopalsamy and C. Gao, *J. Mater. Chem. A,* 2 (2014) 9736.
42. V. Shkirskiy, M. Kang, I.J. McPherson, C.L. Bentley, O.J. Wahab, E. Daviddi, A.W. Colburn and P.R. Unwin, *Anal. Chem.,* 92 (2020) 12509.
43. A.K. Bakhshi and G. Bhalla, *J. Sci. Ind. Res.* 63 (2004) 715.
44. X. Jia, S. Gao, T. Liu, D. Li, P. Tang and Y. Feng, *Electrochim. Acta,* 245 (2017) 59.
45. R.J. Wu, M.Y. Chen, B.H. Hsien, H.N. Luk and M. Chavali, *J. Chin. Chem. Soc.,* 61 (2014).
46. Z.S. Stojanović, E. Mehmeti, K. Kalcher, V. Guzsvány and D.M. Stanković, *Food Anal. Methods,* 9 (2016) 2701.
47. M. Hadi and H. Mostaanzadeh, *Russ. J. Electrochem.,* 54 (2018) 1045.
48. M.B. Gumpu, N. Nesakumar, S. Sethuraman, U.M. Krishnan and J.B.B. Rayappan, *Sens. Actuators, B,* 199 (2014) 330.
49. Y.-T. Lin, C.-H. Chen and M.S. Lin, *Sens. Actuators, B,* 255 (2018) 2838.